ELSEVIER

Volume 220 December 2014 ISSN 0022-4596

JOURNAL OF SOLID STATE CHEMISTRY

IN THIS ISSUE:

Surfactant-thermal method to prepare two novel two-dimensional Mn–Sb–S compounds for photocatalytic applications

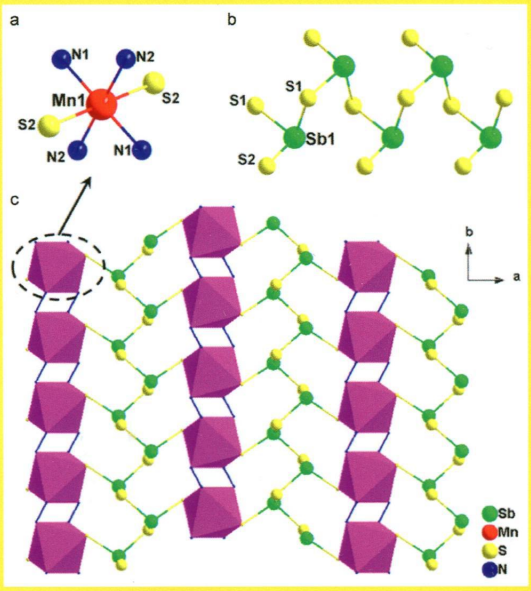

Lina Nie, Wei-Wei Xiong, Peizhou Li, Jianyu Han, Guodong Zhang, Shengming Yin, Yanli Zhao, Rong Xu and Qichun Zhang

Available online at www.sciencedirect.com

ScienceDirect

ELSEVIER

Volume 220, December 2014

JOURNAL OF SOLID STATE CHEMISTRY

www.elsevier.com/locate/jssc

CONTENTS

Abstracted/indexed in BioEngineering Abstracts, Chemical Abstracts, Coal Abstracts, Current Contents/Physics, Chemical, & Earth Sciences, Engineering Index, Research Alert, SCISEARCH, Science Abstracts, and Science Citation Index. Also covered in the abstract and citation database SCOPUS®. Full text available on ScienceDirect®.

Regular Articles

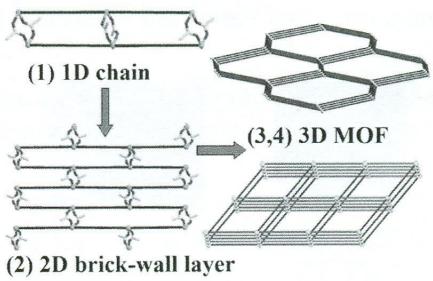

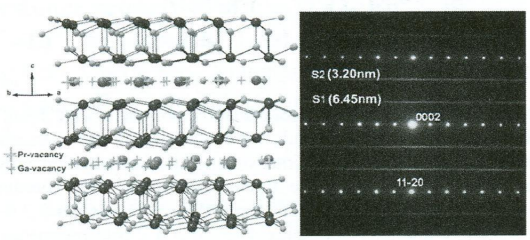

Left: Crystal structure of $Pr_{1.33}Pt_4Ga_{10}$ showing Pr and Ga vacancies in the Pr_2Ga_3 plane. Right: Tunneling electron microscopy (TEM) image of $Pr_{1.33}Pt_4Ga_{10}$. These vacancies have been studied using TEM and pair distribution function analysis. Magnetic measurements reveal that Pr^{3+} ions order ferrimagnetically below 7.8(2) K.

Regular Articles—Continued

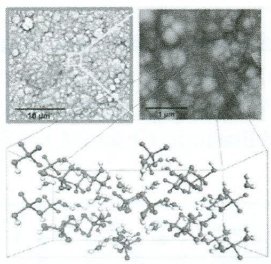

Rhenium oxides were electrodeposited on a copper surface and after environmental aging was formed the $H(ReO_4)H_2O$ compound. The characterization of the synthesized material was made through the comparison of experimental evidence with quantum mechanical computations carried out by means of density functional theory (DFT).

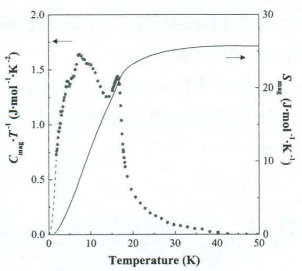

Temperature dependence of the magnetic specific heat divided by temperature (C_{mag}/T) and the magnetic entropy (S_{mag}) for Tb_3RuO_7. Two-step magnetic transition has been observed.

Continued

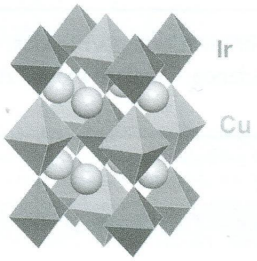

A new member of the $A_2B'B''O_6$ double-perovskite family with JT-active Cu^{II} at the B' site and Ir^{VI} at the B'' site is synthesized through high pressure synthesis and characterized for the structural and magnetic properties.

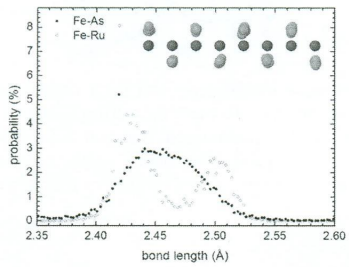

Fe–As and Ru–As bond length distributions as obtained by pair distribution function analysis of $La(Fe_{0.70}Ru_{0.30})AsO$; As atoms (purple spheres) undergo a random shifting around their crystallographic positions (red spheres: Fe/Ru atoms).

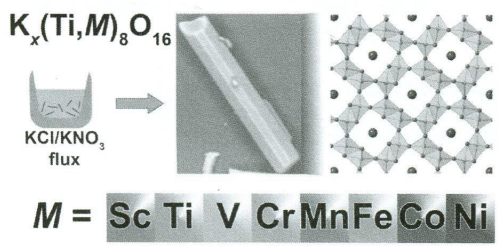

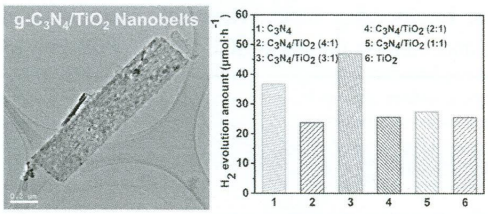

A novel strategy to fabricate the g-C_3N_4/TiO_2 nanobelt (NB) heterostructures was reported. The g-C_3N_4/TiO_2 NB heterostructures exhibited highly effective photocatalytic activities for photodegradation of Rhodamine B and H_2 production.

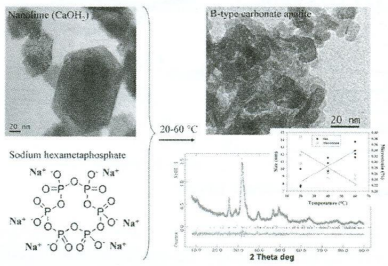

Controlled synthesis of carbonated apatite at moderate temperatures using nanolime and sodiumhexametaphosphate as starting reagent.

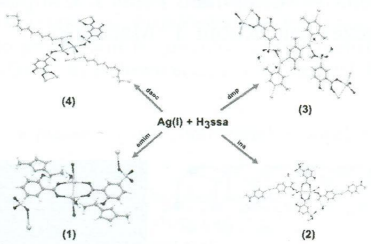

In this study, four new Ag(I)-coordination polymers with 5-sulfosalicylate and some N-donor ligands were synthesized and characterized. Complexes **1** and **2** are one-dimensional (1D) coordination polymers while complexes **3** and **4** are three-dimensional (3D) coordination polymers. Complex **3** consists of three dimensional (3D) 3,3,6-c net with 3,3,6T37 topology. Complex **4** exhibits a 2-fold interpenetrating 3D framework with tfc topology. The complexes **1–4** contain ligand-supported (**1–3**) and unsupported (**4**) argentophilic Ag···Ag interactions. Photoluminescence spectra of the complexes demonstrated that photoluminescent properties may be attributed to intraligand transition of coordinated Hssa ligand.

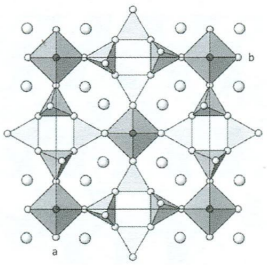

Mixed tetrahedral–octahedral framework of the tetragonal polymorph of $Rb_2Sc[Si_4O_{10}]F$.

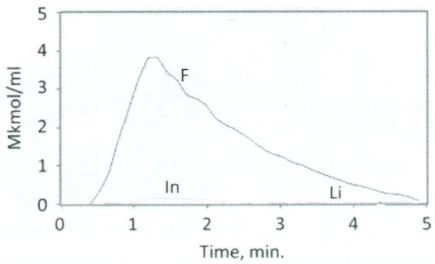

Differential dissolution technique applied for detection of dispersive precipitates in as-grown $LiInSe_2$ single crystals: kinetic curves of the phase dissolution: F is the main phase $Li_{0.96}In_{1.01}Se_2$ (98.9%), secondary minor phases Li_2Se (0.1%), In_2Se_3 (0.9%).

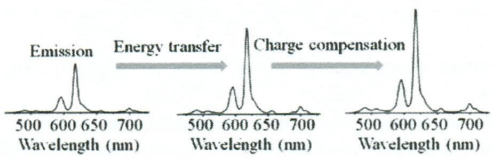

Energy transfer and charge compensation can enhance PL intensity of phosphors obviously

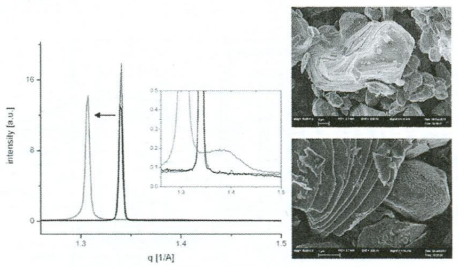

The effect of chemical dedoping of Li_xCoO_2 leads to a significant change in the (003) peak and to exfoliation for x=1/3.

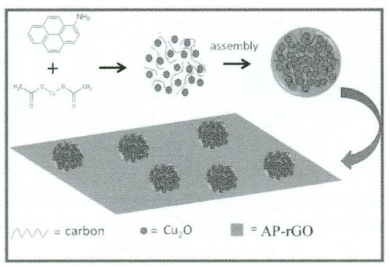

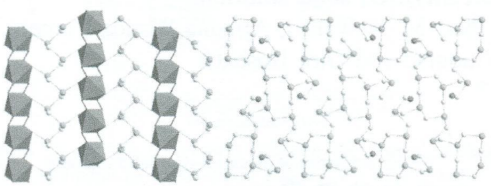

Two novel 2D framework sulfides, $[MnSb_2S_4(N_2H_4)_2]$ (1) and [Mn(tepa)Sb_6S_{10}] (2) (tepa = tetraethylenepentamine), have been successfully synthesized under surfactant-thermal conditions and show active visible-light-driven photocatalytic properties for hydrogen production.

Continued

Exploring the structural and magnetic properties of TiO_2/SnO_2 core/shell nanocomposite: An experimental and density functional study

Pawan Chetri, Priyanka Basyach and Amarjyoti Choudhury

page 124

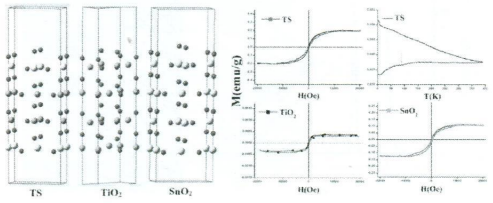

Above pictorial presentation (from left) represents the model for TS, TiO_2 and SnO_2 used for DFT calculation and the obtained magnetic results for all the prepared systems

Growth and characterization of nonlinear optical telluromolybdate $CoTeMoO_6$ single crystals

Mirosław Mączka, Krzysztof Hermanowicz, Andrzej Majchrowski, Łukasz Kroenke, Adam Pietraszko and Maciej Ptak

page 142

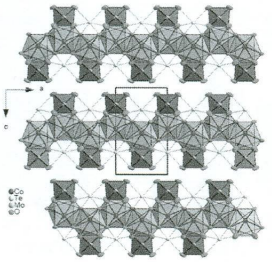

View of $CoTeMoO_6$ crystal structure along the *b*-axis.

Crystal structure and orbital-singlet state of $Ag_xVP_2O_7$

Masashige Onoda and Takuma Sakamoto

page 132

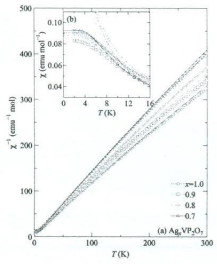

(a) The temperature dependencies of inverse magnetic susceptibilities for $Ag_xVP_2O_7$ with $x = 0.7-1$ and (b) the low-temperature susceptibilities.

A combined experimental and theoretical study of the supramolecular self-assembly of Cu(II) malonate complex assisted by various weak forces and water dimer

Prankrishna Manna, Somnath Ray Choudhury, Monojit Mitra, Saikat Kumar Seth, Madeleine Helliwell, Antonio Bauzá, Antonio Frontera and Subrata Mukhopadhyay

page 149

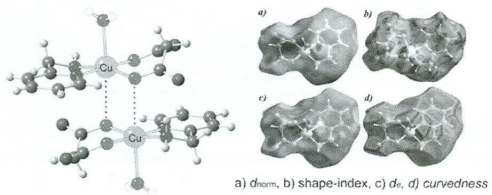

Interplay of weak forces like hydrogen bonding, lone pair···π, Cu···Cu and π–stacking interactions leading to the formation of supramolecular network in $[Cu(C_3H_2O_4)(C_6H_8N_2)(H_2O)]_2{\cdot}4H_2O$ complex.

***Ab initio* calculation of excess properties of $La_{1-x}(Ln, An)_xPO_4$ solid solutions**

Yan Li, Piotr M. Kowalski, Ariadna Blanca-Romero, Victor Vinograd and Dirk Bosbach

page 137

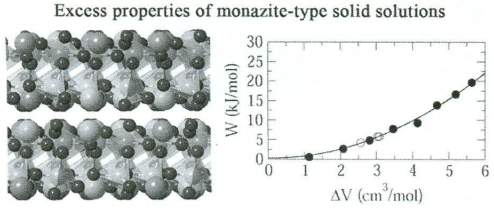

Variations of thermoelectric properties of $Mg_{2.2}Si_{1-y}Sn_{y-0.013}Sb_{0.013}$ materials with different Si/Sn ratios

Hongli Gao, Tiejun Zhu, Xinbing Zhao and Yuan Deng

page 157

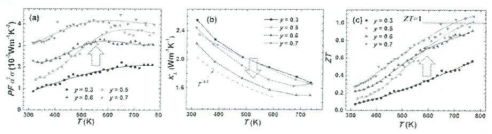

(a) Temperature dependence of power factor of $Mg_{2.2}Si_{1-y}Sn_{y-0.13}Sb_{0.013}$ samples.

(b) Temperature dependence of lattice thermal conductivity of $Mg_{2.2}Si_{1-y}Sn_{y-0.13}Sb_{0.013}$ samples.

(c) Temperature dependence of dimensionless figure of merit *ZT* of $Mg_{2.2}Si_{1-y}Sn_{y-0.13}Sb_{0.013}$ samples.

The interplay of microstructure and magnetism in $La_3Ni_2SbO_9$

Peter D. Battle, Maxim Avdeev and Joke Hadermann

page 163

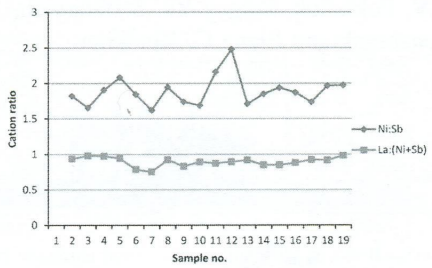

Composition variations across a crystal of $La_3Ni_2SbO_9$ result in anomalous magnetic behavior.

Chromium substitution in mullite type bismuth aluminate: $Bi_2Cr_xAl_{4-x}O_9$ with $0 \leq x \leq 2.0$

Tapas Debnath, Ahamed Ullah, Claus H. Rüscher and Altaf Hussain

page 167

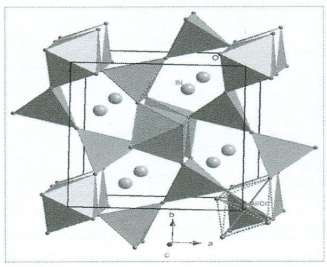

Structural model of Cr doped bismuth aluminate, $Bi_2Cr_xAl_{4-x}O_9$.

Enhanced luminescence properties in $(Sr_{1-x}Ba_x)_{2.97}SiO_3N_{4/3}$:0.03$Eu^{2+}$ oxynitride phosphor

Xia He, Kehui Qiu, Xueguang Lu, Kun Zhao and Zixu Jiang

page 172

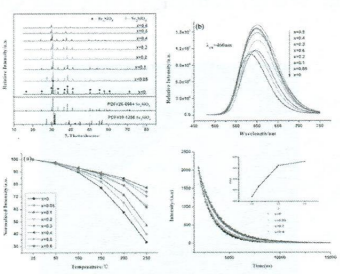

Through the change of micro-structure by doping Ba^{2+} ions proved by the XRD patterns, $(Sr_{1-x}Ba_x)_{2.97}SiO_3N_{4/3}$:0.03$Eu^{2+}$phosphor eventually achieves the extension of lifetime and the improvement of luminescence properties and thermal stability.

Crystal structure and luminescence properties of a novel red-emitting phosphor $BaAlBO_3F_2$:Eu^{3+}

Wanping Chen, Ahong Zhou, Yan Liu, Xiaoyan Dai and Xin Yang

page 177

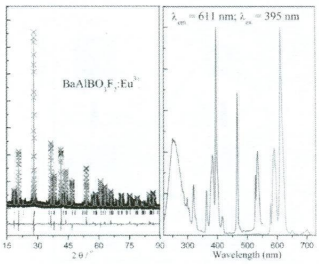

The luminescence behavior and Rietveld refinement of $BaAlBO_3F_2$:Eu^{3+} indicate that the red-emitting phosphor has potential application in white LED and the host has a hexagonal structure with *P*-6 space group.

Transformation of dense AgI into a silver-rich framework iodide using thiophenol as mineralizer

Ren-Chun Zhang, You-Juan Zhang, Bai-Qing Yuan, Jun-Peng Miao, Bao-Hua Pei, Pan-Pan Liu, Jun-Jie Wang and Dao-Jun Zhang

page 185

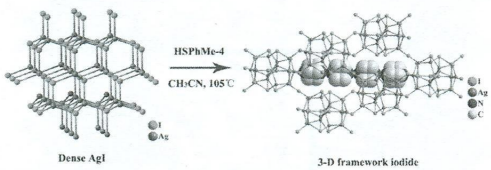

A new 3-D iodoargentate was synthesized by transformation of dense AgI in I^--deficient system using thiophenol as mineralizer.

Electronic polarizability and interaction parameter of gadolinium tungsten borate glasses with high WO_3 content

Yukina Taki, Kenji Shinozaki, Tsuyoshi Honma, Vesselin Dimitrov and Takayuki Komatsu

page 191

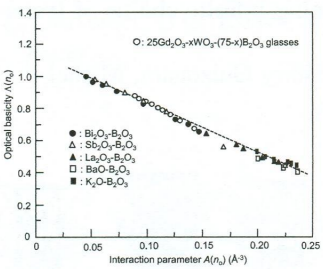

This figure shows the correlation between the optical basicity and interaction parameter in borate-based glasses. The data obtained in the present study for Gd_2O_3–WO_3–B_2O_3 glasses are locating in the correlation line for other borate glasses. These results shown in Fig. 8 clearly demonstrate that Gd_2O_3–WO_3–B_2O_3 glasses having a wide range of optical basicity and interaction parameter are regarded as glasses consisting of acidic and basic oxides.

Continued

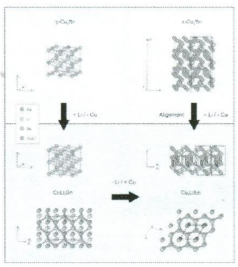

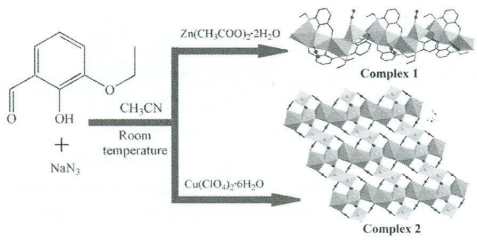

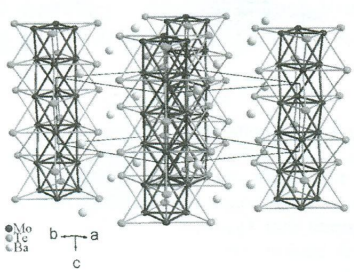

We present here the synthesis, the crystal structure, and the electrical and magnetic properties of the new compound $BaMo_6Te_6$ containing infinite chains of trans-face shared Mo_6 octahedra.

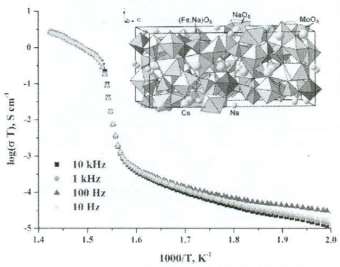

A new triple molybdate $Na_{25}Cs_8Fe_5(MoO_4)_{24}$ was synthesized and structurally characterized, its physicochemical properties were studied.

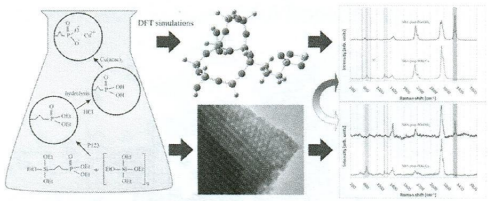

The present study is devoted to mesoporous silica SBA-15 containing propyl-copper phosphonate units. The species were investigated to confirm of synthesis procedure correctness by the micro-Raman technique combined with DFT numerical simulations. Complementary research was carried out to test the structure of mesoporous samples.

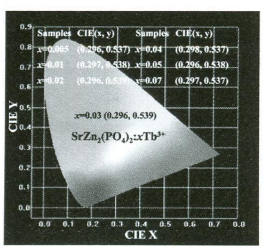

$SrZn_2(PO_4)_2:Tb^{3+}$ can produce green emission under near-UV excitation, and its luminescent properties can be improved by incorporating A^+ (A=Li, Na, and K).

Crystal chemistry and optical investigations of the $Cu_2Zn(Sn,Si)S_4$ series for photovoltaic applications

Mohamed Hamdi, Alain Lafond, Catherine Guillot-Deudon, Faouzi Hlel, Mohamed Gargouri and Stéphane Jobic

page 232

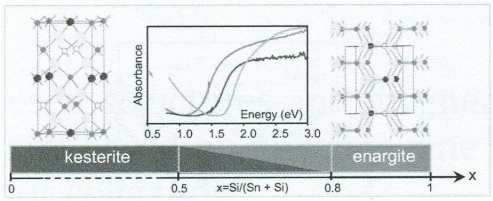

Two solid solutions have been pointed out in the $Cu_2Zn(Sn_{1-x}Si_x)S_4$ series with the kesterite and the enargite type structures.

Influence of Na*X* (*X*=I or Cl) additions on GeS_2–Ga_2S_3 based glasses

A. Bréhault, S. Cozic, R. Boidin, L. Calvez, E. Bychkov, P. Masselin, X. Zhang and D. Le Coq

page 238

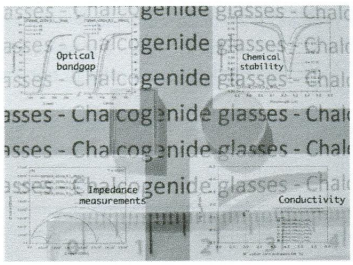

Characterizations of Na*X*–GeS_2–Ga_2S_3 chalcogenide glasses (*X*=Cl or I).

Phase transformations and selective growth in $YMnO_3$ films

I. Iliescu, M. Boudard, O. Chaix-Pluchery, L. Rapenne and H. Roussel

page 245

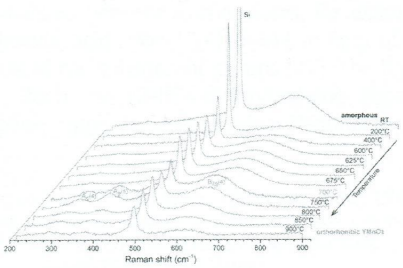

Temperature-dependent Raman spectra of an amorphous as-deposited Y–Mn–O film in the temperature range RT – 900 °C. The red spectrum marks the crystallization of the amorphous phase into the o-$YMnO_3$ phase.

Phase transitions and unusual behavior of heat capacity in metal organic framework compound $Zn_2(C_8H_4O_4)_2{\cdot}N_2(CH_2)_6$

I.E. Paukov, D.G. Samsonenko, D.P. Pischur, S.G. Kozlova and S.P. Gabuda

page 254

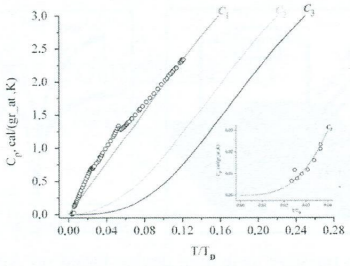

Specific heat C_p is proportional to the first degree of temperature showing a strong anisotropy of crystal vibrations corresponding to 1D continuum in $Zn_2(C_8H_4O_4)_2{\cdot}N_2(CH_2)_6$.

A new anion-deficient fluorite-related superstructure of $Bi_{28}V_8O_{62}$

T. Đorđević and Lj. Karanović

page 259

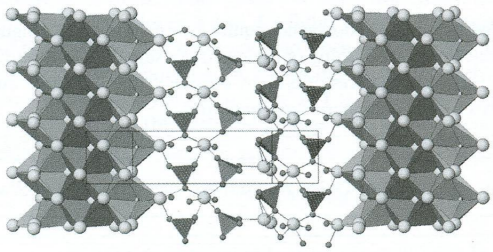

The [$\bar{4}$ 0 1] projection of two slabs and inter-slab part of the structure in one layer parallel to the $(\bar{3}\ 0\ 8) = (0\ 0\ \bar{2})_F$ plane (F in subscript indicate a fluorite type structure). The large green circles are Bi atoms. Small blue circles represent partly and fully occupied O sites, respectively. Pink (hatched black) are $V1O_4$ and blue (hatched white) are $V2O_4$ coordination tetrahedra.

Monoclinic distortion and magnetic coupling in the double perovskite $Sr_{2-x}Ca_xYRuO_6$

P.L. Bernardo, L. Ghivelder, G.G. Eslava, H.S. Amorim, I. Felner and S. Garcia

page 270

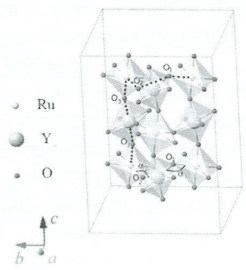

Tilting of the oxygen octahedra in $Sr_{2-x}Ca_xYRuO_6$ due to strong monoclinic distortions.

Continued

Rapid Communications

A light-modified ferroelectric resistive switching behavior in Ag/$BaMoO_4$/FTO device at ambient temperature

W.X. Zhao, B. Sun, Y.H. Liu, L.J. Wei, H.W. Li and P. Chen

page 32

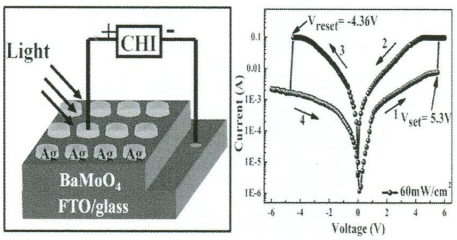

We fabricate a resistive switching device based on Ag/$BaMoO_4$/FTO, the device shows superior white-light controlled bipolar resistive switching memristive characteristics.

Effect of the introduction of oxide ion vacancies into cubic fluorite-type rare earth oxides on the NO decomposition catalysis

Toshiyuki Masui, Ryosuke Nagai and Nobuhito Imanaka

page 181

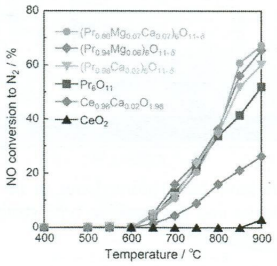

Oxide anion vacancies intentionally introduced into the cubic fluorite-type lattice bring about positive effect on NO decomposition catalysis.